SCANNING ELECTRON MICROSCOPY/1983/IV (Pages 1535-1545)
SEM Inc., AMF O'Hare (Chicago), IL 60666 USA

0586-5581/83$1.00+.05

# X-RAY FLUORESCENCE ANALYSIS IN THE SCANNING ELECTRON MICROSCOPE WITH A MASSIVE ANODE

Richard Eckert

Standard Elektrik Lorenz AG, Stuttgart

(Paper received March 23 1983, Complete manuscript received August 15 1983)

## Abstract

XRF in the SEM offers a possibility of analysing materials without a surface metallization, but with detection limits in the low ppm range. The rigid construction with a massive anode and an independent filter foil presented here is also suitable for routine applications. The necessary actions involved when changing from the usual electron excitation method to XRF are mainly reduced to replacing the sample holder carrying the XRF construction.

KEY WORDS: Counting rate, detection limit, filter foil, fluorescence analysis, massive anode, peak to background ratio, trace analysis, X-ray analysis, X-ray fluorescence.

Address for correspondence:
Richard Eckert
Research Centre, Standard Elektrik Lorenz AG,
Hirthstr. 42, D-7000 Stuttgart 40, W. Germany
Phone No. (0711) 8214017

## Introduction

Usually the characteristic X-rays of a sample in the scanning electron microscope (SEM) are generated directly by striking the sample surface with the electron beam. When registrating the X-rays with a spectrometer a nondestructive material analysis is executed within a few minutes. The positionable fine electron beam permits a high local resolution together with a very small detectable mass (about $10^{-12}$ g).

On the other hand, electron excitation is relatively insensitive to measure low concentrations. Here, in the case of uniformly distributed traces the weak X-ray signals of traces are overlayed by large amounts of continuous radiation ("bremsstrahlung") from the main material. The bremsstrahlung will hide these weak signals in its statistical fluctuations, resulting in minimum detectable concentrations of about a half per mille (500 ppm) of the main material. Of course, the electron bremsstrahlung is generated by deceleration of the striking electrons on the sample surface. The liberation of bremsstrahlung is therefore inherently coupled with the method of direct electron excitation.

Illuminating the sample with high energy X-rays will also generate the characteristic sample X-rays, but without the electron bremsstrahlung. Now traces are easily detectable. This method has been well-known as X-ray fluorescence analysis (XRF) for 55 years /6/. Therefore, the main task would be to transmit the sophisticated methods of XRF /8/ to the analysis work in the SEM. The application of XRF to the SEM would enlarge the possibilities of analysis for the SEM-user. Lower detection limits, greater information depth, as well as material analysis without interfering surface metallization are the benefits of X-ray fluorescence in the SEM.

## Fluorescence in the SEM with a Foil Anode

Historically, the first successful fluorescence setup in the SEM was made with a foil anode /12/. This setup transfers the low current transmission X-ray tube /9, 24/ to the SEM. As can be seen from Fig. 1, the electron beam strikes the surface of a metal foil. There, at a depth of typically 1 µm, the electrons generate X-radiation.

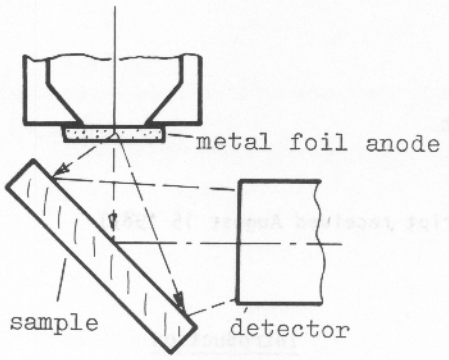


Fig. 1: Setup with foil anode

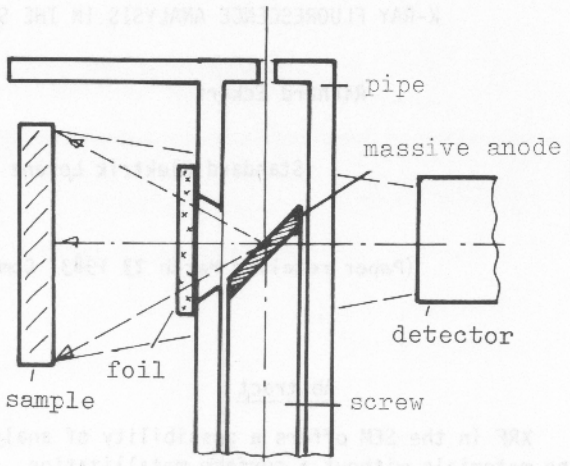


Fig. 2 a: Setup with massive anode (side view)

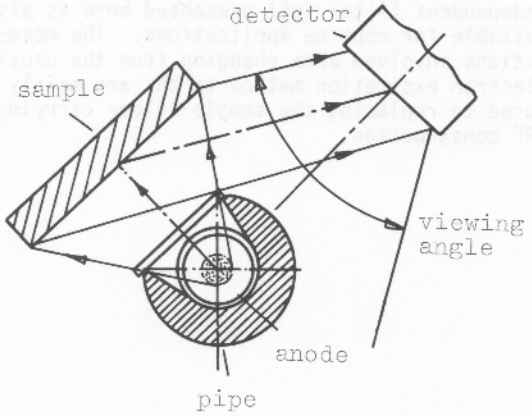


Fig. 2 b: Setup with massive anode (top view)

The X-rays penetrate the remaining part of the foil and illuminate the sample. Obviously, the mechanisms of X-ray emission and electron absorption are coupled in the same foil. Especially in the case of low energy X-rays both conditions together can only be achieved to a limited degree: The foil has to absorb all impinging electrons, but should transmit a sufficient amount of the generated X-rays. A thin foil will be penetrated by the electrons, a thicker foil will absorb the low energy radiation. Nevertheless, several authors report of a much higher signal to background ratio than to electron excitation for elements with atomic numbers of Z = 20 to 40 /11, 14, 15, 21, 22/. Corresponding to this, the minimum detectable concentration for traces reaches $c_{mdl}$ = 9 ppm, e.g. rubidium and strontium in glass /12/.

## Fluorescence in the SEM with a massive Anode

In Fig. 2 a and 2 b the construction with a massive anode is illustrated. As reported previously /4, 5/, the electron beam is directed onto a small sheet of metal, the massive anode. The anode is fixed on the upper side of a screw, adjustable in height and direction. On the anode screw rests a metal pipe with a small opening on its top for the incoming electrons and a large window at its side directed to the sample for the emerging X-rays. The window is closed by a metallized plastic foil or by a metal foil. The pipe thus acts as a Faraday cage, absorbing all incoming electrons. A horizontal plate on the top of the pipe reaching over the sample, protects it against stray electrons from the primary beam as well as against stray radiation. The sample is then illuminated only by the X-rays from the anode. The sample X-rays pass beside the pipe and fall on a Si(Li)-detector. The detector is usually directed to the axis of the electron beam so that only a part of the detector viewing angle is utilized by the X-ray emitting sample. In the spectrometer EDAX 950 used, a magnetic trap behind the detector window limits the detector viewing angle horizontally to nearly $10^{o}$. Resulting from the electron beam-detector distance of 11 cm, a maximum sample area of 1 $cm^2$ can be examined.

A wedge-shaped flange between detector and SEM would turn the detector axis to the middle of the sample, allowing a smaller distance and a correspondingly higher counting rate with a moderate electron current. But the construction also works without a wedge flange and without the need to modify the equipment.

An interesting setup with a massive anode but without the filter has been published before /7/. Since the sample was not protected against reflected electrons, the success was only limited. However, this setup also clearly demonstrates the benefits of using a massive anode.

The construction presented generates the X-rays mainly in the massive anode and absorbs the electrons and the low energy part of the X-radiation in the foil. Unlike in the case of the anode foil, here the functions of emission, absorption and transmission are mostly independent. The construction with a massive anode operates like a conventional X-ray tube, with the exception that

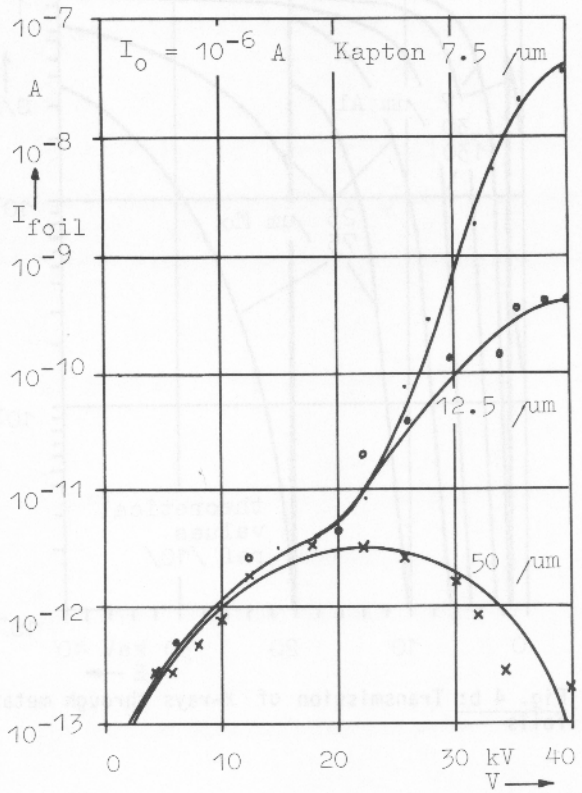


Fig. 3 a: Current across plastic filter foils (Kapton$^R$)

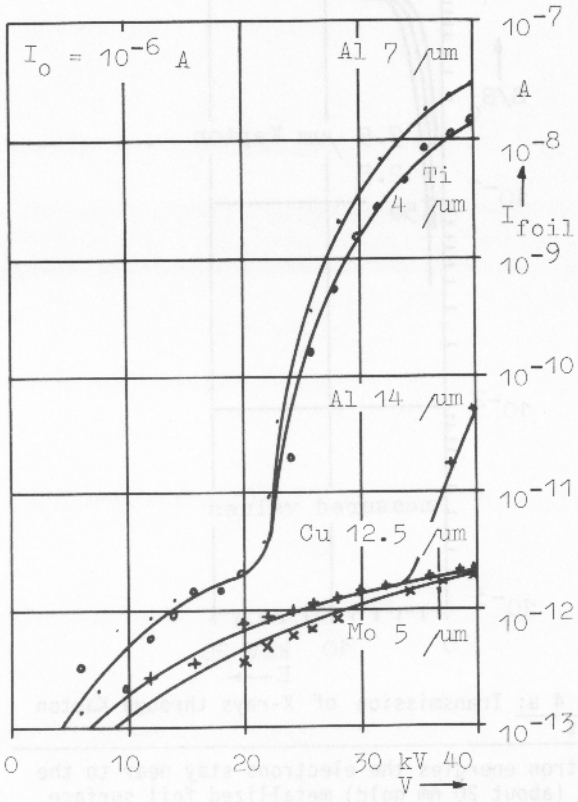


Fig. 3 b: Current across metal filter foils

here many different anode materials can be used (nearly all metals). In addition, the filter foils are available in various materials with different foil thicknesses /13/. Anode, filter pipe and a sample holder are mounted on a ground plate. With the sample inserted, the construction is shut by a cap preventing stray electrons and stray radiation from the SEM walls to reach the sample. An exchange of sample, filter or anode is accomplished quickly and without difficulty. The ground plate is fixed on a common sample holder, so that a change in the analysis method reduces the effort mainly to changing the sample holder in the SEM.

## Electron Absorption by the Foil

To absorb all impinging high energy electrons, a minimum thickness of the filter foil is required. The product of the needed filter thickness and the density is nearly independent of the foil material used but increases with the electron energy /2, 3/. Usually, the extrapolated penetration depth is given by an empirical formula

$$R_E = a \cdot E^n \qquad (1)$$

$R_E$ = penetration depth in µg/cm$^2$
$E$ = electron energy in keV
$a$ = empirical constant in the order of 7 to 12
$n$ = empirical exponent in the order of 1.3 to 1.7

With the formula in the energy range of 10 to 100 keV as given in /3/

$$R_E = 10 \cdot E^{1.43} \qquad (2)$$

typical foil materials with a thickness of a few microns should absorb all electrons, see Table 1.

Table 1: Calculated penetration depth for electrons

| Material | Density g/cm$^3$ | $R_E$ at 20 keV µm | $R_E$ at 40 keV µm |
|---|---|---|---|
| Kapton$^R$ | 1.42 | 5.1 | 14.0 |
| aluminum | 2.70 | 2.7 | 7.2 |
| titanium | 4.51 | 1.6 | 4.3 |
| copper | 8.96 | 0.8 | 2.2 |
| molybdenum | 10.20 | 0.7 | 1.9 |

In contrast to this, Fig. 3 a and 3 b give the measured electron current across different foils. Here the construction was attached in the SEM with a Faraday cage in the place of the sample. A primary beam current of about 20 µA was set. The electrons penetrating the foil and reaching the cage were measured by a microammeter. The curves, normalized to $I_o$ = 1 µA, exhibit an ohmic part in the low current range to $I_{foil} \leq$ 1 pA, probably caused by a leakage current in the setup. In the higher range, the current across the foil grows exponentially. Noteworthy in Fig. 3 a is the curve of the 50 µm Kapton foil. Here the current across the foil exhibits a maximum for electron energies of 30 keV. A further increase in the energy will reduce the current. With low

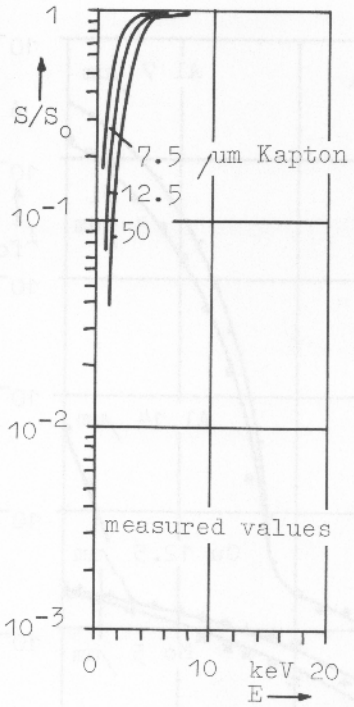


Fig. 4 a: Transmission of X-rays through Kapton foils

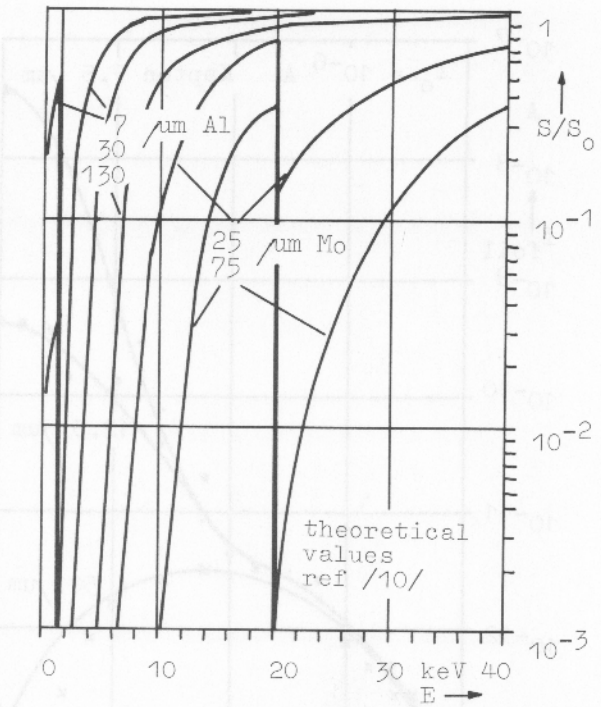


Fig. 4 b: Transmission of X-rays through metal foils

electron energies the electrons stay near to the thin (about 20 nm gold) metallized foil surface. An increase in the energy will enlarge the penetration depth, and cause a space charge in the foil material.

The electrons reaching the sample will generate bremsstrahlung. A current across the foil must therefore be ruled out. Foils of 4 µm titanium, 7 µm aluminum or 50 µm Kapton for example can only be used up to electron energies of $E \leq 20$ keV.

## X-Ray Transmission by the Foil

All foils will absorb a part of the anode radiation. If a higher absorption is desired, metal foils are better suited than plastic foils /10, 20/. For a larger absorption it is favorable to use a more absorbing material of moderate thickness than a thicker material with weak absorption. The reason is the scattering of X-rays in the foil material. This scattering depends mainly on the product of thickness and density, not on the material itself. Scattered radiation will illuminate the surroundings of the sample instead of the sample itself, enlarging the spectrum background by reflections. Fig. 4 a and 4 b represent the transmission across foils of different thicknesses. As can be seen, low energy radiation is strongly absorbed and high energy radiation only to a negligible degree. This simple correlation has the important feature of filtering the anode radiation (see below, Filtered Excitation).

## Counting Rate

The counting rate S of an X-ray emitting sample measured by the detector in a fixed

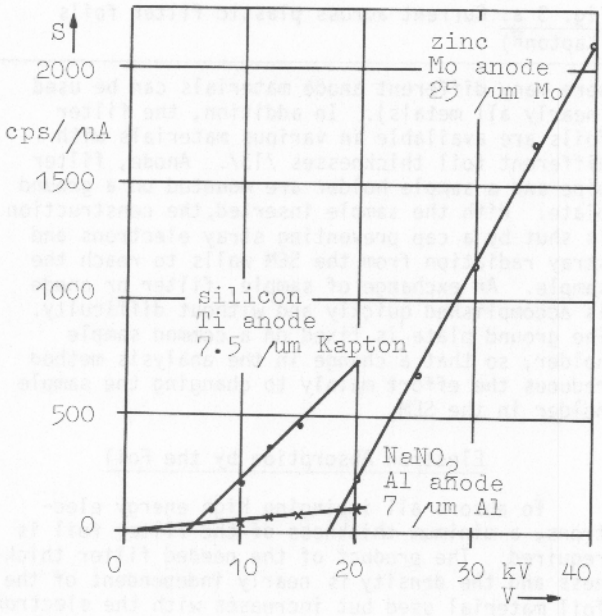


Fig. 5: Counting rates at the Si(Li) detector

position will grow linearly with the illuminated sample area. To get a reasonable counting rate, the sample area should be as large as possible. In the construction presented here the area should amount to 1 cm$^2$. The counting rate is proportional to the electron beam current $I_0$ and to the difference between the electron energy E and the absorption energy of the anode material $E_{abs}$.

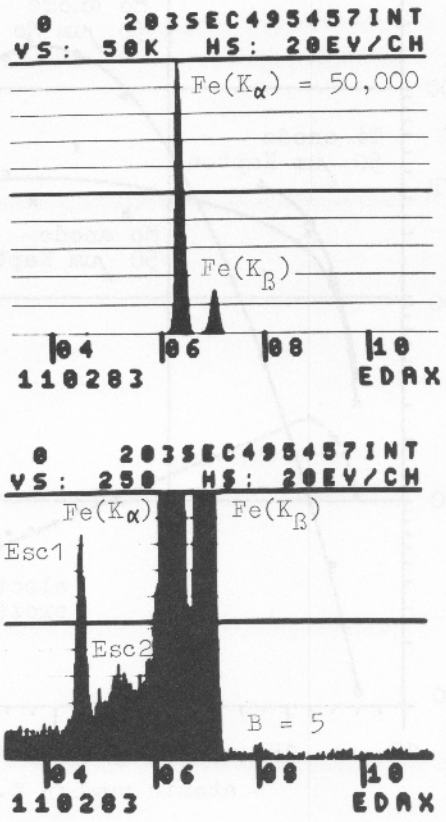


6 a

6 b

Fig. 6 a and 6 b: Spectrum of iron. Molybdenum anode with 50 µm molybdenum filter, 30 kV, 5 min analysis time. a: vertical full scale 50,000 counts, b: vertical full scale 250 counts.

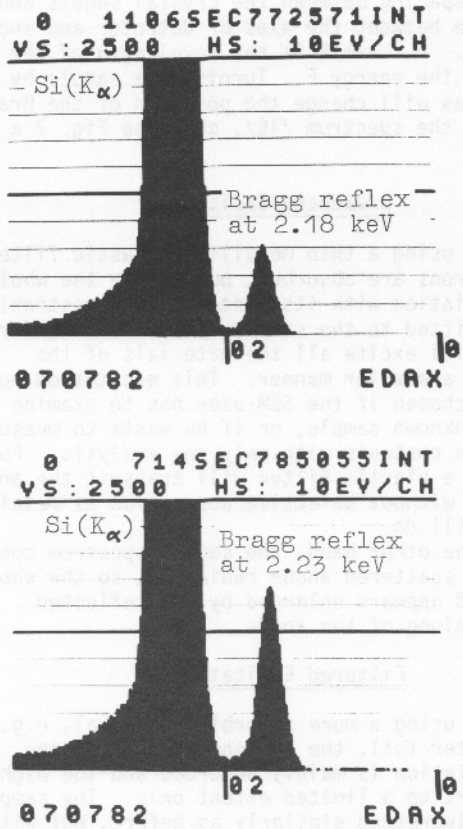


7 a

7 b

Fig. 7 a and 7 b: Spectrum of silicon with Bragg reflex. Titanium anode with 7.5 µm Kapton filter, 20 kV, 20 min analysis time. Turning the sample a few degrees will change height and position of the reflex.

Thus,

$$S = b \cdot I_o \cdot (E - E_{abs}) \qquad (3)$$

Due to the limitation of the beam current in a SEM it is often more advantageous to use a higher electron energy instead of trying to further increase the current. Fig. 5 illustrates several examples for the counting rate S, measured in counts per second (cps) and µA beam current.

## The Fluorescence Spectrum

A fluorescence spectrum contains much less X-ray background compared with an electron excited spectrum. Fig. 6 a and 6 b represent the spectrum of iron, excited by a molybdenum anode with a 50 µm molybdenum filter. Here also small signals can be seen clearly. Beside the strong Fe($K_\alpha$) and Fe($K_\beta$) lines the escape peaks at 4.66 and 5.32 keV are visible. The escape peaks are caused by fluorescence excitation of the silicon in the detector with the characteristic iron lines. Furthermore, the sum peaks of 2 x Fe($K_\alpha$) and Fe($K_\alpha$) + Fe($K_\beta$) at 12.80 and 13.46 keV can be observed. Such sum peaks are generated by counting two incoming X-ray quanta as one with the accumulated energy by the detector. While both pairs of lines are also present in an electron excited spectrum, here in the fluorescence spectrum they are clearly visible by the reduced background /16/. Further, the reflected anode radiation is always present. With an applied beam voltage of 30 kV the molybdenum lines at 17.44 and 19.60 keV can be observed, too. Generally, a characteristic line of the anode radiation is accompanied by a broad Compton peak on the low energy side. Compton peaks are caused by inelastic scattering of the anode radiation in the sample material, and their intensity will grow for low atomic numbers of the sample. Also, in such a sample the low energy part of the background appears enlarged. The whole spectrum thus looks similar to a bath tub. This is the same as occasionally observed in usual SEM analysis when unintentional indirect excitation occurs. Here, a part of the sample will obstruct the free view from the tested area to the detector.

In the middle region of the spectrum the background is low. In this region traces can be easily detected, with higher detection sensitivity in the part near the anode radiation.

If a monocrystalline sample is illuminated by unfiltered radiation, further lines are visible. Here the anode X-rays at different energies fulfil Bragg's law

$$n \cdot \lambda = 2 \cdot d \cdot \sin \vartheta \qquad (4)$$

with d = spacing between the crystal sheets and $2\vartheta$ = angle between the axes of detector and anode radiation. $\lambda = c \cdot h/E$ is the wavelength of the X-rays with the energy E. Turning the sample by a few degrees will change the position of the Bragg reflex in the spectrum /16/, see also Fig. 7 a and 7 b.

## Broadband Excitation

When using a thin metallized plastic filter, all electrons are absorbed, but nearly the whole anode radiation with its content of bremsstrahlung is transmitted to the sample. Such broadband radiation will excite all the materials of the sample in a similar manner. This excitation mode is to be chosen if the SEM-user has to examine a totally unknown sample, or if he wants to measure all of the contents with only one analysis. Furthermore, a plastic filter will transmit the anode radiation without selective absorption as metal filters will do.

On the other hand, the sample spectrum contains the scattered anode radiation, so the whole background appears enlarged by the reflected bremsstrahlung of the anode.

## Filtered Excitation

When using a more absorbing material, e.g. a metal filter foil, the low energy part of the anode radiation is mainly absorbed and the high energy part to a limited extent only. The sample is then fluoresced similarly as before, but with a low background in the interesting part. The filtered radiation gives best results in detecting trace elements for a particular energy range. As in usual XRF, the best excitation is achieved with an exciting energy only a little higher than the absorbing energy of the trace /1, 2/. Therefore, the SEM-user will mostly choose the filtered radiation in trace analysis.

## The Peak to Background Ratio

The ratio net peak height divided by the X-ray background beside the peak determines the detectability of an element. Pure elements exhibit an electron excited P/B = 20 to 200. Fluorescence excitation should lead to a much higher P/B. As can be seen from Fig. 6, the net peak height Fe($K_\alpha$) of the represented iron spectrum amounts to P = 50,000 counts. The background on the right, high energy side of the peak amounts to B = 5 counts, resulting in a P/B = 10,000. The enlarged background on the left, low energy side, stems mostly from the detector /17, 18, 19/. Even if using a radioisotope as an X-ray source, e.g. Fe 55, for spectrometer calibration, SEM-analysts will observe such "tailing" of peaks. Consequently, here for the calculation of P/B the undisturbed background on the high energy side of the peak is used.

Fig. 8 presents the measured ratios P/B for pure elements. Obviously, the broadband radiation excites a number of elements in a similar manner. So the P/B stays nearly constant for these elements. In contrast to this, the filtered radiation excites some elements excellently but others

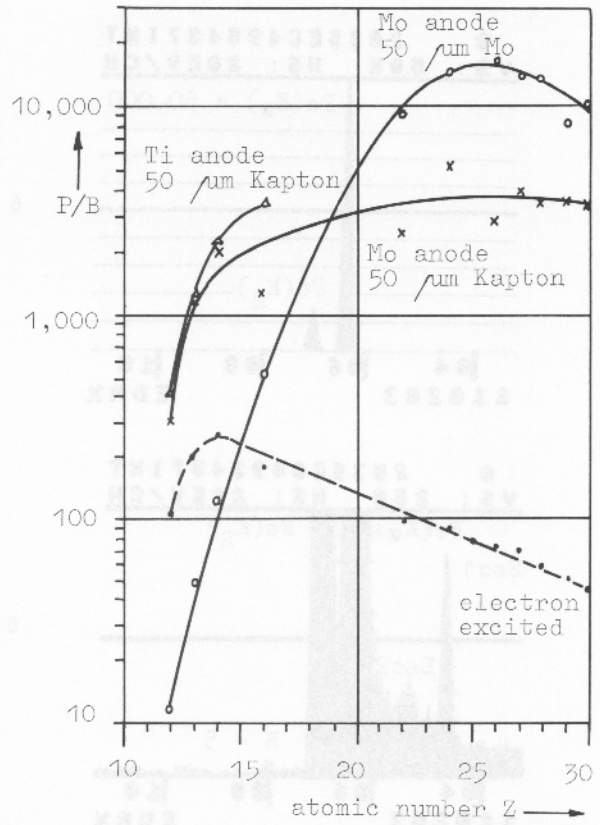


Fig. 8: P/B-ratio versus atomic number Z at 20 kV. Upper part: Fluorescence excitation. Lower part: Electron excitation.

to a limited degree only. The corresponding P/B-curve therefore exhibits a relatively sharp maximum with a steep decline towards lower atomic numbers. Fig. 8 also contains measured values with electron excitation. Here, with a much higher background, the mean values of the background between both sides of the peaks were taken. An electron excited P/B = 60 is typical, compared with a broadband fluorescence excited $P/B_{fl} = 3{,}000$ and a filter excited $P/B_{fl} = 10{,}000$. With both XRF modes, $P/B_{fl}$ declines sharply towards lower atomic numbers. This is mostly caused by the decreasing fluorescence yield for light elements and the complementary, increasing yield for emitted Auger electrons. Nevertheless, even sodium exhibits when fluoresced a much better P/B than it does with electron excitation.

Fig. 9 shows the spectrum of sodium in $NaNO_2$. The sodium has electron excited $P/B_{el} = 18.4$. The same material, fluoresced with an aluminum anode, exhibits a $P/B_{fl} = 665$. Thus, the $P/B_{fl}$ is 36 times the $P/B_{el}$. In the similar case of sodium in glass (Fig. 10) with $P/B_{el} = 1.6$ and $P/B_{fl} = 29$ XRF generates an 18 times higher P/B than electron excitation. The fairly high $P/B_{el}$ is probably caused by an inner fluorescence of the sodium by silicon. For low atomic numbers ($Z \leq 9$, fluorine) the fluorescence method is limited by the decreasing counting rate (Fig. 5). Already in the case of sodium in $NaNO_2$ the counting rate for V = 10 kV decreases in the given construction to

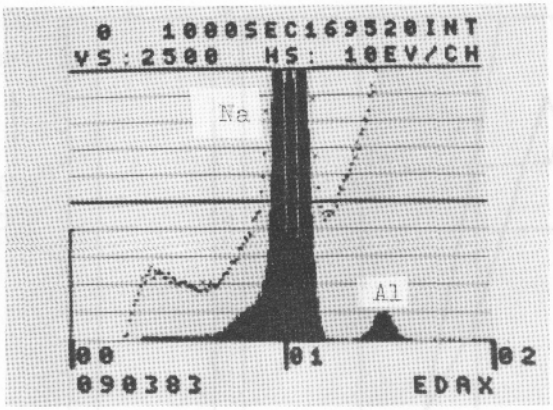


Fig. 9: Spectrum of $NaNO_2$. Analysis time 20 min. Massive: Aluminum anode with 7 µm aluminum filter at 10 kV, $P_{Na}$ = 13,690, B = 20.6. At 1.49 keV the reflected peak Al($K_\alpha$) is visible. Points: Electron excited spectrum at 20 kV, $P_{Na}$ = 20,260, B = 1,000.

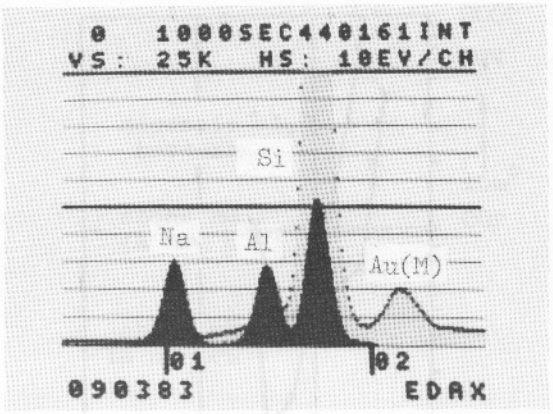


Fig. 10: Spectrum of glass NBS 612. Analysis time 20 min. Massive: Aluminum anode with 7 µm aluminum filter at 10 kV, $P_{Na}$ = 3,200, B = 110. Points: Electron excited spectrum at 20 kV. At the right the gold peak from surface metallization can be seen. $P_{Na}$ = 1,360, B = 840.

9 cps/µA in the Na($K_\alpha$)-peak, thus necessitating a correspondingly long analysis time. Therefore, it seems generally advantageous to adhere to the practice used up to now, i.e. to excite the elements from carbon to fluorine (Z = 6 to 9) in the SEM by electrons.

## Strategy for Trace Analysis

In the case of an unknown sample the SEM-user will choose as a first step the broadband excitation. As a second step, to compare the traces with the contents of a reference material, the filtered excitation would be applied. As shown in Fig. 11 a and 11 b, anode and filter should be selected such that the exciting radiation will reasonably excite the traces, but not the main material of the sample. Thus, a larger part of the whole counting rate will arise from the wanted traces. So the limited counting rate, applicable to energy dispersive spectrometers (usually 2,000 cps), will be profitably used. The exciting radiation should be only slightly higher than the absorbing energy of the trace. In addition, in the case of $E_{abs\ trace} < E_{abs\ material}$, the energy of the anode radiation should be lower than the absorption energy of the main material.

As mentioned before, the XRF spectrum exhibits a constant low background in the middle region. This background will enlarge linearly to the high energy part caused by the reflected anode radiation /21/. Best sensitivity for trace detection would be achieved for traces with emission lines in the low background region nearby the anode reflex, say on the edge of the growth. The best sensitivity is reached when using a set of suitable anodes and filters and proceeding along the following lines (values given for example in /10/):

1. Which is the emission energy of the wanted trace?
2. Which filter has at this energy a transmission of only $S/S_{o\ trace} = 0.01$?
3. Which anode has with this filter for its characteristic line a transmission of $S/S_{o\ anode}$ = 0.3 to 0.4?

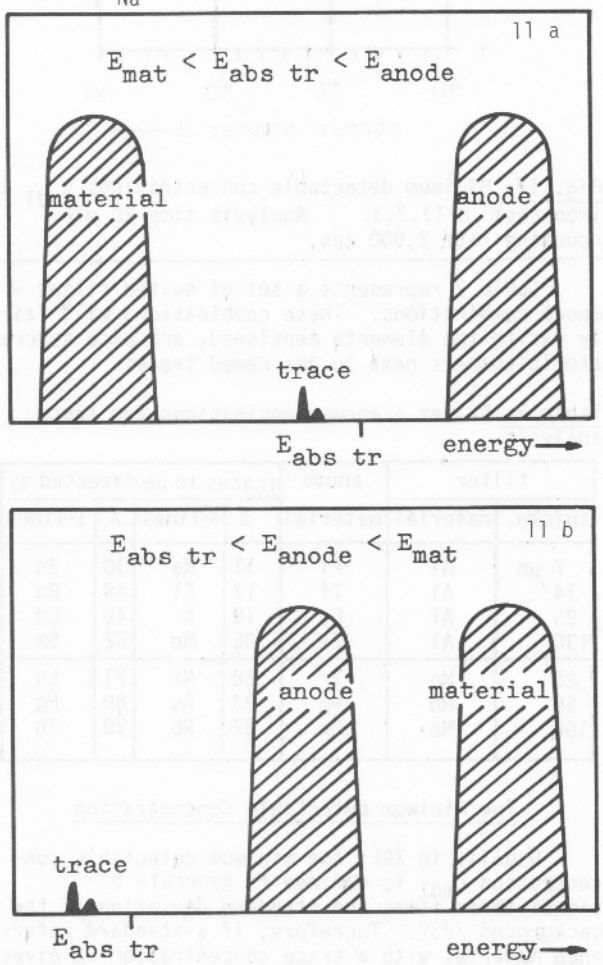


Fig. 11 a and 11 b: Strategy for trace analysis. a: If $E_{mat} < E_{abs\ tr}$, the energy of the anode radiation should be only a little higher than $E_{abs\ tr}$. b: If $E_{abs\ tr} < E_{mat}$, the energy of the anode radiation should be in the range between them.

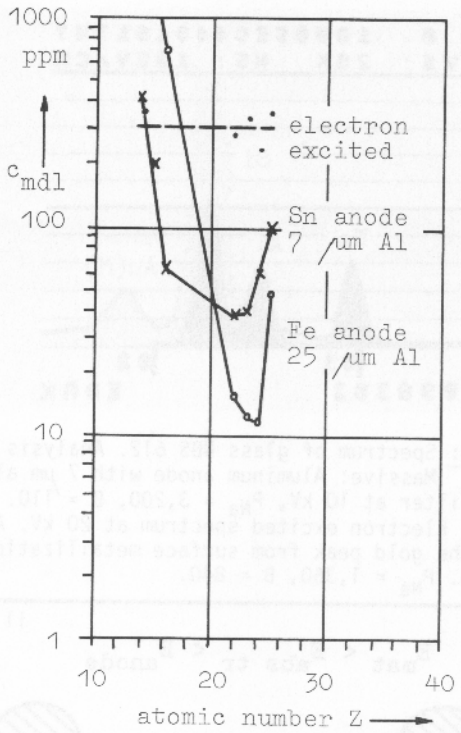


Fig. 12: Minimum detectable concentrations $c_{mdl}$ in iron cast 8FT1,2,3. Analysis time 20 min, counting rate 2,000 cps.

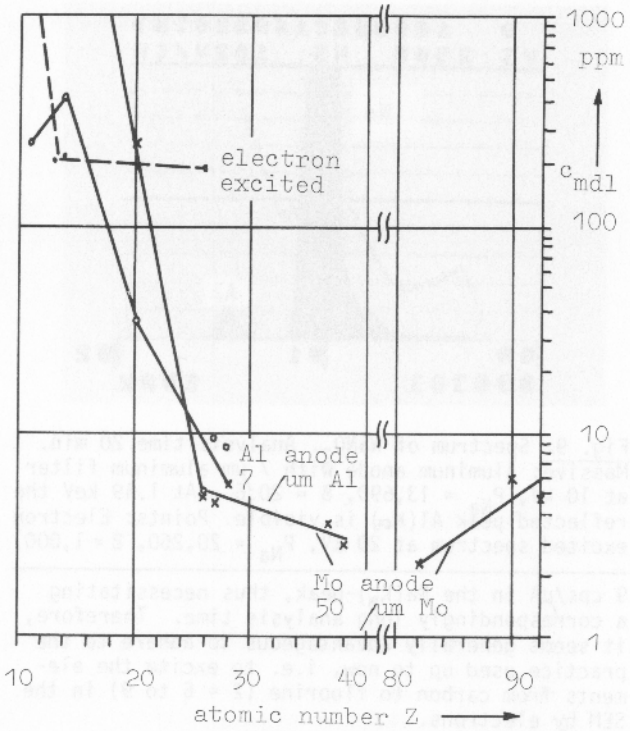


Fig. 13: Minimum detectable concentrations $c_{mdl}$ in glass NBS 612. Analysis time 20 min, counting rate 2,000 cps.

Table 2 represents a set of suited filter - anode combinations. These combinations will fairly excite the elements mentioned, and also several atomic numbers next to the named traces.

Table 2: Filter - anode combinations for trace analysis

| filter | | anode | traces to be detected by | | | |
|---|---|---|---|---|---|---|
| thickn. | material | material | Z | K-lines | Z | L-lines |
| 7 µm | Al | Al | 11 | Na | 30 | Zn |
| 14 | Al | Ti | 17 | Cl | 44 | Ru |
| 25 | Al | Fe | 19 | K | 48 | Cd |
| 130 | Al | Zr | 25 | Mn | 62 | Sm |
| 25 | Mo | Zr | 28 | Ni | 71 | Lu |
| 50 | Mo | Mo | 33 | As | 80 | Hg |
| 100 | Mo | Mo | 37 | Rb | 90 | Th |

## The Minimum detectable Concentration

Usually in XRF, the minimum detectable concentration $c_{mdl}$ is defined to generate a signal three times the standard deviation of the background /23/. Therefore, if a standard reference material with a trace concentration $c_o$ gives a net signal $(N - N_B)$, it is possible to calculate the minimum detectable concentration

$$c_{mdl} = \frac{3\sqrt{N_B}}{(N - N_B)} \cdot c_o \qquad (5)$$

$N_B$ = number of the background counts of the standard
$N$ = total counts in the characteristic line of the standard
$c_o$ = trace concentration in the standard.

The mentioned energy interval for optimum sensitivity is to be set /23/ 1.2 times the full width at half maximum (FWHM) in the line. With a FWHM = 159 eV at Mn($K_\alpha$) the optimum energy interval would amount to 190 eV. To avoid a peak overlap here, a smaller interval of only 140 eV was taken. Fig. 12 depicts electron and XRF excited spectra of a certified iron standard. The electron excited $c_{mdl}$ amounts to $c_{mdl\,el}$ = 370 ppm independent of the trace element. This is caused by the low electron penetration depth of only about 1 µm. Here, the radiation of different traces stems from the same 1 µm surface layer with only weak absorption. In contrast to this, the $c_{mdl}$ curve for XRF declines with the atomic number increasing. According to Moseley's law /2/, elements with high atomic numbers radiate with corresponding high energies

$$E = R \cdot (Z - 1)^2 \left(1 - \frac{1}{n^2}\right) \qquad (6)$$

R = 13.6 eV (Rydberg constant)
n = 2: $K_\alpha$
n = 3: $K_\beta$

The high energy radiation of these elements penetrates the sample. The fluorescence radiation stems therefore from deeper sheets of the material.

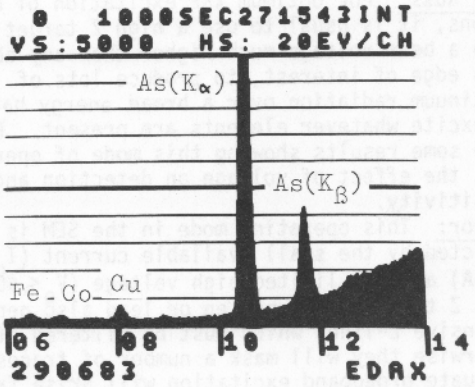


Fig. 14: Spectrum of silicon, doped with 2,000 ppm arsenic. Molybdenum anode with 50 µm molybdenum filter at 35 kV. The signals of iron, cobalt and copper stem from the surroundings, probably the filter pipe and the detector housing.

The excitation volume is greater, resulting in a strong X-ray signal and a low $c_{mdl}$. Because of this an excitation of the high energy K-lines is generally preferable to that of L-lines of the same trace. Obviously, the $c_{mdl}$ depends on the matrix, i.e. the surrounding main material.

The iron cast (Fig. 12) results in $c_{mdl}$ = 50 to 13 ppm, depending on the excitation condition.

Fig. 13 represents the $c_{mdl}$ curve for NBS glass. Here, with a light matrix, the electron excited minimum concentration amounts constantly to $c_{mdl\ el}$ = 200 ppm. With XRF, the curve falls from $c_{mdl}$ = 400 to 40 ppm for traces with Z = 11 to 20 (Na to Ca) and stays nearly constant with $c_{mdl}$ = 2 to 7 ppm for traces of Z ≥ 24 (Cr).

Fig. 14 shows as an example the spectrum of an arsenic doped silicon wafer. Here, with an arsenic concentration of about $c_o$ = 2,000 ppm, $N_B$ = 2,974, and $N_{As}$ = 90,058 results a $c_{mdl}$ = 3.6 ppm arsenic in silicon.

## Conclusions

The presented construction with a massive anode offers new possibilities of trace analysis to SEM-users. With an independent choice of anode and filter material together with a choice of filter thickness, peak to background ratios of P/B = 3,000 to 10,000 can be achieved, depending on the excitation conditions. This corresponds to detection limits in the low ppm range.

## Acknowledgement

The author greatly appreciates the contribution of L. M. Middleman and J. D. Geller.

## References

/1/ Birks LS. (1964). Excitation of characteristic X-rays by protons, electrons, and primary X-rays. J. Appl. Phys. 35, 2578-2581.

/2/ Birks LS. (1971). Electron probe microanalysis. Chemical Analysis 17, 2nd Ed. Wiley Interscience, NY, 107.

/3/ Drescher H, Reimer L, Seidel H. (1970). Rückstreukoeffizient und Sekundärelektronen-Ausbeute von 10-100 keV-Elektronen und Beziehungen zur Raster-Elektronenmikroskopie. Z. Angew. Phys. 29, 331-336.

/4/ Eckert R. (1982). Ein Röntgenfluoreszenz-Zusatz für die Spurenanalyse. Beitr. elektronenmikr. Direktabb. Oberfl. 15/1, G. Pfefferkorn (ed), Verlag Remy, Münster, W-Germany, 41-48.

/5/ Eckert R. (1982). X-ray fluorescence in the SEM with a stub target. 10th Intern. Congr. on Electron Microscopy, Deutsche Ges. f. Elektronenmikroskopie (ed), 1, 677-678.

/6/ Glocker R, Schreiber H. (1928). Quantitative Röntgenspektralanalyse mit Kalterregung des Spektrums. Ann. der Physik 85, 1089-1102.

/7/ Gould RW, Healey JT. (1975). Secondary fluorescent excitation in the scanning electron microscope: Improved sensitivity of energy dispersive analysis. Ref. Sci. Instrum. 46, 10, 1427-1428.

/8/ Herglotz HK, Birks LS (ed). (1978). X-ray spectrometry. Practical Spectroscopy 2, Marcel Dekker, NY.

/9/ Jaclevic JM, Giauque RD, Malone DF, Searles WL. (1972). Small X-ray tubes for energy dispersive analysis using semiconductor spectrometers. Advances in X-ray Analysis 15, Plenum Press, NY, 266-275.

/10/ Jenkins R, De Vries JL. (1969). Practical X-ray spectrometry. App. I: Table of mass-absorption coefficients. 2nd Ed. Macmillan, London.

/11/ Linnemann B, Reimer L. (1978). Comparison of X-ray elemental analysis by electron excitation and X-ray fluorescence. Scanning 1, 109-117.

/12/ Middleman LM, Geller JD. (1976). Trace element analysis using X-ray excitation with an energy dispersive spectrometer on a scanning electron microscope. Scanning Electron Microsc. 1976; I: 171-178 and 762.

/13/ Plannet W. (1983). X-ray source. AGAR-catalog No 4, 74. Plano GmbH, Friedrichsplatz 9, 355 Marburg, W-Germany.

/14/ Pozsgai I. (1982). Energy dispersive X-ray fluorescence analysis in the scanning electron microscope, 10th Intern. Congr. on Electron Microscopy. Deutsche Ges. f. Elektronenmikroskopie, Frankfurt, W. Germany, 1, 681-682.

/15/ Riessen A, Terry KW. (1982). X-ray induced X-ray fluorescence in a JSM-35C scanning microscope. JEOL News 20 E 3 (75), JEOL Ltd., 19-23

/16/ Russ JC. (1976). Erroneous peaks in energy dispersive X-ray spectra. Advances in X-ray analysis 19, Plenum Press, NY, 161-165.

/17/ Russ JC. (1977). Processing of energy dispersive X-ray spectrum. X-ray Spectrometry 6, 1, 37-55.

/18/ Russ JC. (1977). Resolving spectrum interferences using non-gaussian peaks. EDAX EDitor 7, 3, 12-16.

/19/ Sanders WM, Holm DM. (1969). An analytical method for unfolding gamma-ray spectra. Los Alamos Scientific Lab., Los Alamos, N.Mex., Rept.LA-4030.

/20/ Vane RA, Stewart WD. (1980). The effective use of filters with direct excitation of EDXRF. Advances in X-ray analysis 23, Plenum Press, NY, 231-239.

/21/ Warren JB, Kraner HW. (1982). Optimized stage design for X-ray fluorescence analysis in the scanning electron microscope. Scanning Electron Microsc. 1982; IV: 1373-1378.

/22/ Weiss RM. (1979). Erhöhung der Nachweisempfindlichkeit bei der qualitativen Röntgenanalyse im REM durch Röntgen-Fluoreszenz Anregung, Beitr. elektronenmikroskop. Direktabb. Oberfl. 12/1, G. Pfefferkorn (ed), Verlag Remy, Münster, W-Germany, 209-216.

/23/ Woldseth R. (1973). X-ray energy spectrometry. Kevex Corp., Burlingame, Ca.

/24/ Zulliger HR, Stewart JE. (1975). X-ray fluorescence analysis with transmission target tubes. Advances in X-ray analysis 18, Plenum Press, NY, 278-287.

## Discussion with Reviewers

J. B. Warren: The construction seems to be mainly a modification of the transmission foil of Middleman and Geller /12/. What are the major differences?
Author: The constructions differ mainly in the part behind the foil. The optical path is quite different, similar to light optics between a glass lensed refractor and a mirror telescope. Here in XRF, the advantage of a massive anode is the independent choice of anode and filter, together with a rigid construction.

I. Pozsgai: How did you measure peak and background for the determination of detection limits?
Author: Most spectrometers display the number of counts in a preset energy range ("energy window"). Hence one window is to be set on the peak to get N, and one on each side close to the peak to get a mean $N_B$.

I. Pozsgai: What spectral contamination can be found in a blind spectrum of 20 min?
Author: Such peaks are generated in those parts of the construction illuminated by primary X-rays. At the time of writing, these are a copper peak from the filter pipe and a smaller iron - cobalt peak from a magnet electron trap inside the Si(Li)-detector. The three peaks are visible in Fig. 14, spectrum of an arsenic doped silicon wafer. If low absorbing materials are to be examined, these should be fixed on a thin plastic foil rather than on a sample holder /21/. So the wafer of Fig. 14, if mounted on an aluminum sample holder, exhibits a signal of lead, too, contained as a trace in the aluminum holder.

J.C. Russ: For optimum XRF excitation of unknowns, it is usual to use a high Z target element with a beam voltage much higher than any absorption edge of interest, to produce lots of continuum radiation over a broad energy band to excite whatever elements are present. Please give some results showing this mode of operation, and the effect of voltage on detection and sensitivity.
Author: This operating mode in the SEM is restricted by the small available current ($I_0 \leq 10\ \mu A$) and the limited high voltage ($V_0 \leq 40$ kV). High Z targets as tungsten or lead also generate intensive L-lines which must be filtered off. Otherwise they will mask a number of traces. An adequate broadband excitation will arise from a medium Z target and a thin metal or plastic filter. So a molybdenum anode with a 14 µm aluminum filter will fairly excite most elements. Table 3 lists the $c_{mdl}$ values of a certified aluminum silicon alloy. The combination of a molybdenum anode with a 25 µm aluminum filter will excite the traces, but not the main material.

Table 3: $c_{mdl}$ of a AlSi standard V1001/2 at different voltages. Mo anode with 25 µm Al filter, 2,000 cps, analysis time 20 min.

| Voltage | Trace | | $c_{mdl}$/ppm | | | Counting rate |
|---|---|---|---|---|---|---|
| kV | Ti | Mn | Fe | Zn | Sr | cps/µA |
| 20 | 17 | 18 | 12 | 10 | 20 | 105 |
| 30 | 30 | 21 | 13 | 11 | 5.4 | 410 |
| 40 | 39 | 20 | 13 | 11 | 4.2 | 740 |

The enlarged sensitivity for high Z traces applying a higher voltage is caused by the intensive $Mo(K_\alpha)$ = 17.44 keV which is then generated. The same causes the linear growth of the counting rate (see also Fig. 5).

J.C. Russ: Quantitative analysis requires constant source/sample/detector geometry and beam current. Have you any data on reproducibility (especially versus specimen change, as in comparing a standard to an unknown)?
Author: This problem is coupled with the choice of a suited standard. The reference standard should consist of the same main material as the sample (glass, ceramics, steel) and contain the same traces. If the trace signals of sample and standard are always related to a main signal, fluctuations of the beam current will not affect the result. Generally, the reproducibility is influenced by counting statistics for trace concentrations near to $c_{mdl}$ as well as by local concentration variations in the standard and the sample. This influence is in XRF much smaller than with electron excitation because of the larger excitation volume, but is still mostly present. Thus, the difference between two measurements on the same side of a standard amounts to about only a fifth of the difference when measuring the front and then the back of this standard.

J. B. Warren: Please show an electron excited spectrum of the arsenic-doped Si wafer used in Fig. 14. For equal counting times, what are the peak-to-background ratios for the electron and the X-ray excited spectrum?
Author: The spectrum given in Fig. 15 was taken at the same high voltage, counting rate, and analysis time as used for the spectrum in Fig. 14. The XRF spectrum contains a net signal of $P_{As}$ = 11,500 and a mean B of B = 330, resulting in a $P/B_{fl}$ = 34.85. With electron excitation, the net signal is $P_{As}$ = 65 only, and the mean B = 373, so $P/B_{el}$ = 0.17. By this, XRF generates here a 200 times higher P/B than electrons directly.

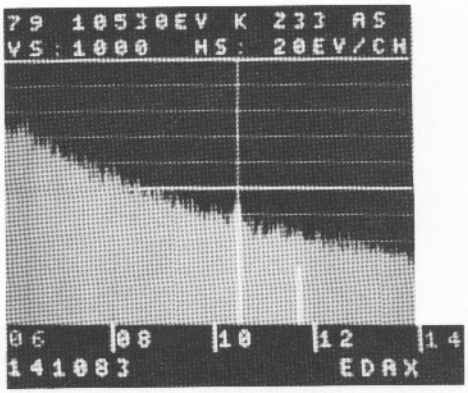


Fig. 15: Electron excited spectrum of an arsenic-doped silicon wafer. V = 35 kV, counting rate 2,200 cps, analysis time 20 min.